ACS APPLIED MATERIALS & INTERFACES

Research Article

www.acsami.org

$LiMn_2O_4$ Surface Chemistry Evolution during Cycling Revealed by *in Situ* Auger Electron Spectroscopy and X-ray Photoelectron Spectroscopy

Ching-Yen Tang,[†] Kevin Leung,[‡] Richard T. Haasch,[§] and Shen J. Dillon*[,†,§]

[†]Department of Materials Science and Engineering, University of Illinois Urbana−Champaign, Urbana, Illinois 61801, United States

[‡]Sandia National Laboratories, MS 1415, Albuquerque, New Mexico 87185, United States

[§]Materials Research Laboratory, University of Illinois Urbana−Champaign, Urbana, Illinois 61801, United States

Supporting Information

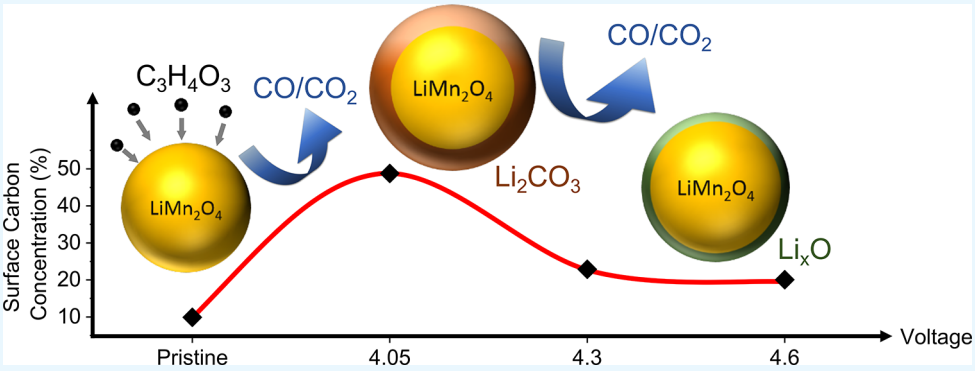

ABSTRACT: This work utilizes *in situ* electrochemical and analytical characterization during cycling of $LiMn_2O_4$ (LMO) equilibrated at different potentials in an ultrahigh vacuum (UHV) environment. The LMO reacts with organic molecules in the vacuum to form a high surface concentration of Li_2CO_3 (≈50% C) during initial charging to 4.05 V. Charging to higher potentials reduces the overall Li_2CO_3 concentration (≈15% C). Discharging to 3.0 V increases the Li_2CO_3 concentration (≈30% C) and over discharging to 0.1 V again reduces its concentration (≈15% C). This behavior is reproducible over 5 cycles. The model geometry utilized suggests that oxygen from LMO can participate in redox of carbon, where LMO contributes oxygen to form the carbonate in the solid electrolyte interphase (SEI). Similar results were obtained from samples cycled *ex situ*, suggesting that the model *in situ* geometry provides reasonably representative information about surface chemistry evolution. Carbon redox at LMO and the inherent voltage instability of the Li_2CO_3 likely contributes significantly to its capacity fade.

KEYWORDS: *$LiMn_2O_4$, cathode material, surface reactions, Li-ion battery, in situ X-ray photoelectron spectroscopy (XPS), in situ Auger electron spectroscopy (AES)*

INTRODUCTION

Lithium-ion battery cycle life imposes a major cost impediment on their deployment in mid to large-scale energy storage, such as electric vehicles and grid scale load leveling.[1,2] Lifetime and maintenance are critical considerations in such applications and it has been an ongoing challenge to find scalable cost-effective solutions that dramatically extend battery cycle life.[3,4] Most capacity fade generally results from so-called side reactions or the physical isolation of active particles. The latter can result from particle fracture, or loss of electronic or ionic percolation to the rest of the system.[5−8] Side reactions describe any process not associated with the primary Li redox reaction, such as Li trapping in nonactive regions, loss of active electrode material, gas evolution, electrolyte decomposition, and chemical reactions with packaging and current collectors.[9−11] While the particular side reactions dominating capacity fade vary with electrode and electrolyte chemistry, the nature of surface chemistry and surface reactions underlies almost all of the potential side reactions. The formation of solid electrolyte interphase (SEI) on electrode surfaces presents challenges to developing a fundamental understanding of surface reactions in Li-ion systems.[12] SEI formation is complex due to the fact that it can result from electrolyte decomposition associated with its instability at the applied potential, a chemical reaction at the inorganic surface that is independent of the electrolyte, catalytic decomposition of the electrolyte, or a chemical reaction between the electrode and electrolyte.[11,13,14] The relative importance and contributions of these various factors to SEI formation and stability remain unclear. The structure and chemistry of the SEI are complex, spatially heterogeneous, and

Received: July 17, 2017
Accepted: September 13, 2017
Published: September 13, 2017

DOI: 10.1021/acsami.7b10442
ACS Appl. Mater. Interfaces 2017, 9, 33968−33978

difficult to characterize.[15] SEI formation also causes the electrode surface, which is of particular interest, to become a buried interface that is challenging to characterize by traditional surface sensitive techniques. Here, we seek to utilize an idealized Li ion battery architecture to study the fundamental surface reactions associated with spinel lithium manganese oxide ($LiMn_2O_4$ or LMO) during cycling, overcharging, and overdischarging. These surface reactions provide a basis for understanding SEI formation and will provide new insights into SEI evolution during cycling.

A number of experimental and computational investigations of LMO SEI formation, structure, and chemistry have been reported.[16−22] Ellipsometry suggests the formation of a ca. 1.5−1.65 nm SEI layer is present after exposure to carbonate based electrolyte and subsequent electrochemical cycling.[16] Delithiating to voltages >4.4 V also alters the near surface crystal structure and chemistry that transforms to Mn_3O_4-like material.[17] *In situ* Fourier transform infrared (FTIR) spectroscopy of LMO in ethylene carbonate (EC) -diethyl carbonate (DEC) based electrolyte indicates that during delithiation C═O and C—O—C peak intensities increase rapidly between 3.9 and 4.2 V, after which they steadily decrease with increasing voltage.[18] This differs from the response of the same electrolyte polarized against Pt, where similar peaks begin to emerge at 4.2 V and increase in intensity with increasing voltage.[18] The formation of SEI on LMO has primarily been attributed to electrolyte instability and decomposition.[18−20] However, the stark difference in the potential dependence of electrolyte decomposition on Pt versus LMO suggests that LMO surface reactions or catalysis must be a major driving force for SEI formation. Density functional theory (DFT) calculations find that, thermodynamically, EC reaction with even fully discharged $LiMn_2O_4$ (i.e., LMO at low voltage) is favorable.[23] EC decomposition is predicted to be kinetically attainable on (100) surfaces in a variety of surface configuration in both a partially charged and fully discharged state.[21] Similar results were calculated for the stability of EC on (111) surfaces, on which no transition metal ion is exposed, unlike the (100) surface.[22] This work did find that EC decomposition is more favorable in the charged state than the discharged state.

This work explores the hypothesis that the SEI chemistry and stability is sensitive to the surface chemistry of LMO in the presence of a C source by cycling a model LMO based battery whose surfaces are exposed to ultrahigh vacuum ($\approx 10^{-8}$). Hydrocarbons and electrolyte vapor present in the vacuum can equilibrate with the LMO during potentiostatic charging and discharging. We explore the surface chemistry and chemical bonding states via *in situ* Auger electron spectroscopy (AES) and X-ray photoelectron spectroscopy (XPS) at different states of charging, overcharging, and overdischarging. AES provides single particle surface chemical bonding state information, which is often inferred from finger printing methods, due to its sensitivity to the core level energy, multiple outer shell energies, and their ionization. This information is also exploited to gain insights into the Mn oxidation states at different potentials in order to better understand SEI stability and the mechanisms for Mn(II) dissolution. XPS provides information about chemical bonding that can be interpreted and quantified more directly than AES, but suffers from lower spatial resolution.

In situ experiments are critical for investigating surface chemistry and oxidation state, which is very sensitive to atmospheric exposure. An *in situ* open electrochemical cell was previously developed based on vacuum stable ionic liquids.[24−26] A thin carbon film on which the electrode particles sit acts as a barrier to direct contact with the electrolyte. However, Li ions and electrons can diffuse through this carbon film allowing for complete electrochemical percolation of all active species. Figure 1 presents a schematic of the experimental testing

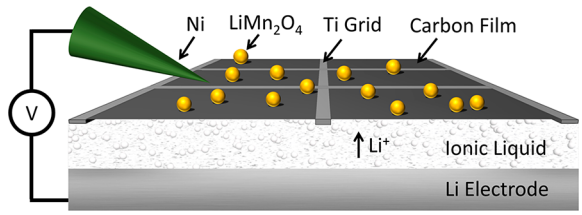

Figure 1. Schematic of *in situ* open electrochemical cell design.

configuration. Our prior work demonstrated that this platform can be used to acquire surface compositional information from AES and XPS during cycling of CuO anodes.[25] AES is particularly useful for Li-ion systems because it can quantify Li composition well at a single particle level. AES's ability to provide chemical bonding information for Li-ion electrodes has not been demonstrated or exploited to date. In this work, we extend this novel approach to investigate the role of applied potential and state of charge on the surface chemistry of LMO equilibrated in an ultrahigh vacuum. We tested a range of different overcharging and overdischarging conditions in order to understand the surface chemistry under both extremes. The results are rationalized in context of DFT predictions for relevant reactions.

EXPERIMENTAL PROCEDURE

***In Situ* Cell Preparation.** The spinel $LiMn_2O_4$ particles were purchased from Sigma-Aldrich, and were dispersed into ethanol at ≈1.0 wt %. The solution was drop cast onto a 400 mesh carbon (≈20 nm) coated titanium TEM grid (Ted Pella, Inc.) and dried at 510 °C on a hot plate (Corning) for 10 min in the Ar-filled glovebox (LABstar, MBRAUN) with oxygen and water concentrations <0.5 ppm. The *in situ* cell was also assembled in the glovebox. The grid supported $LiMn_2O_4$ served as the cathode, which rested on top of either 10 wt % LiTFSI (bis(trifluoromethane)sulfonimide lithium salt) in $P_{13}TFSI$ (1-methyl-1-propylpyrrolidinium bis-(trifluoromethanesulfonyl)imide) or 10 wt % $LiBF_4$ in EMI-BF_4 (1-ethyl-3-methylimidazolium tetrafluoroborate) soaked Whatman fiberglass separator, which was placed on a piece of lithium metal (1.5 mm in thickness) (Sigma-Aldrich). The lithium counter electrode was connected to the stainless steel current collector. A nickel coated bronze metal served as the contact to the working electrode. The cells were sealed in an airtight jar prior to transfer to the AES and XPS chambers.

***Ex Situ* Testing.** The $LiMn_2O_4$ electrodes were prepared by mixing 80 wt % of $LiMn_2O_4$ powder (Sigma-Aldrich), 10 wt % of carbon black (Sigma-Aldrich) and 10 wt % of poly(vinylidene fluoride) (PVDF; Sigma-Aldrich) in *N*-methylpyrrolidone (NMP; Sigma-Aldrich) solvent. The mixed slurry was coated onto aluminum foil and dried in the oven at 80 °C for 24 h. The electrode disks were then punched out of the coated foil sheets. A Swagelok cell prepared from a $LiMn_2O_4$ cathode and a Li metal anode was assembled in an argon-filled glovebox. One M $LiPF_6$ dissolved in ethylene carbonate and dimethyl carbonate (1:1 wt/wt; Novolyte Technologies) and a polypropylene membrane (25 μm in thickness, Celgard 2500) were the electrolyte and separator, respectively. Individual samples were equilibrated at a given potential for 2 h. The cells were then disassembled and then washed in dimethyl carbonate. These samples were analyzed by AES in order to compare with the *in situ* results.

DOI: 10.1021/acsami.7b10442
ACS Appl. Mater. Interfaces 2017, 9, 33968−33978

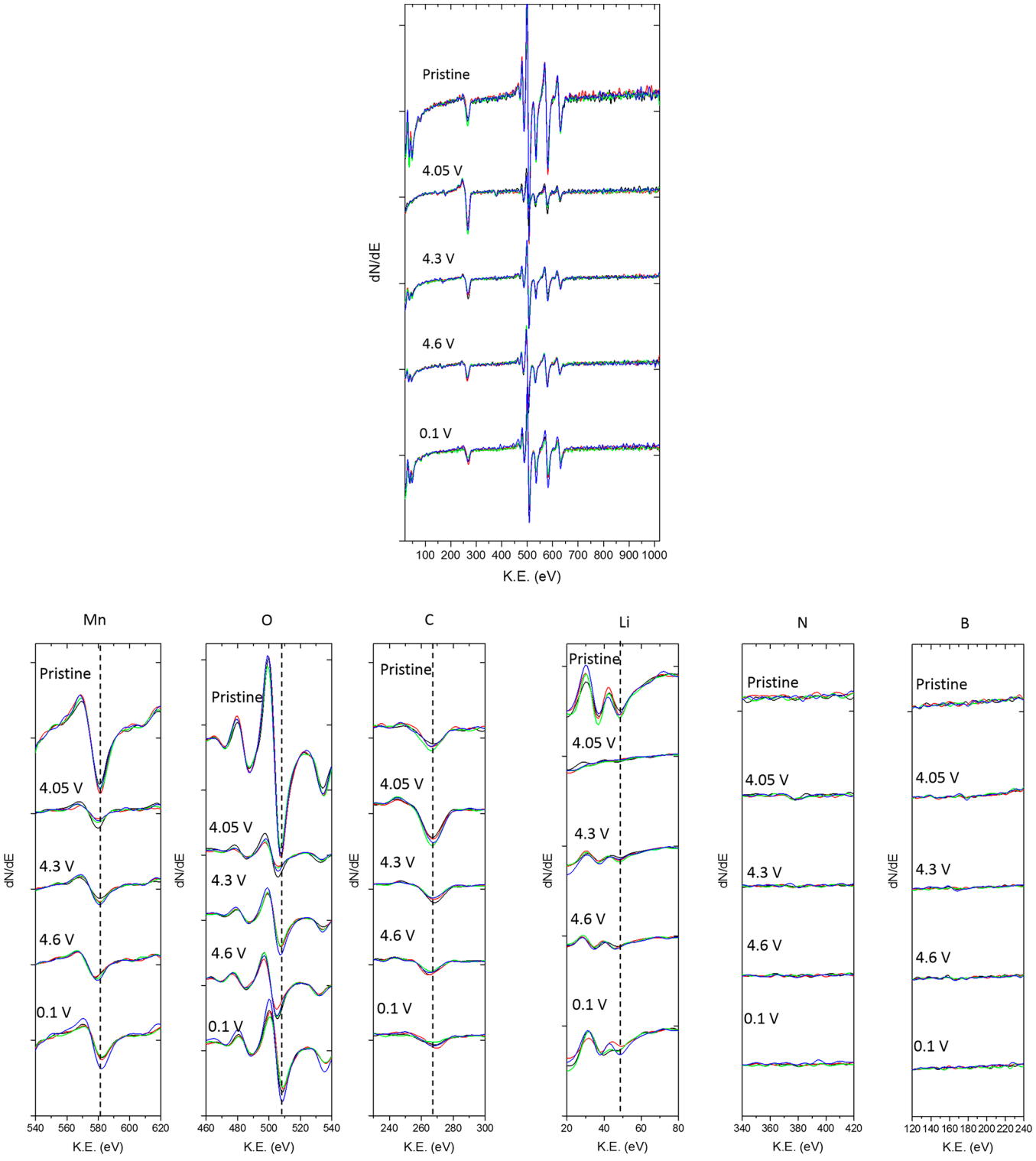

Figure 2. $LiMn_2O_4$ AES spectra obtained at different potentials. Each line represents a distinct particle. High-resolution spectra of Mn, O, C, Li, N, and B at different voltage steps were also shown, the dotted lines are included as guides intersecting minima associated with the pristine materials.

Electrochemical Measurements. Potentiostatic charge and discharge were carried out by using a digital potentiostat (SP200, Biologic Co.) connected to either the AES or the XPS systems in a 2-electrode configuration.

***In Situ* AES Analysis.** Auger electron spectroscopy (AES) measurements were carried out in an ultrahigh vacuum chamber with the PHI 660 scanning Auger microprobe. The vacuum pressure of the chamber remained at 1×10^{-8} Torr. Acquisitions were performed with a 3 keV primary electron beam and a 2.4 mm objective aperture which resulted in an approximately 350 nm spot size. Each spectrum was averaged over 25 cycles in the energy range from 20 to 1020 eV with measurements binned into 0.1 eV channels. Auger data was analyzed by using Multipak software. Auger peak energies are dependent on proper alignment of the zero energy peak, which can lead to small, <1 eV, variations between samples from separate experiments. However, within a single sample tested *in situ* the experimental scatter due to the alignment of the instrument should be considerably lower.

DOI: 10.1021/acsami.7b10442
ACS Appl. Mater. Interfaces 2017, 9, 33968−33978

***In Situ* XPS Analysis.** X-ray photoelectron spectroscopy (XPS) measurements were obtained on a Kratos Axis Ultra X-ray photoelectron spectrometer using monochromatic Al Kα radiation (hυ = 1486.6 eV) as the primary excitation source. The source beam size is 2 mm × 2 mm and the size of the analyzed region is 0.3 mm × 0.7 mm. The instrument vacuum was maintained at 8×10^{-8} Torr during the experiments. The spectrometer was calibrated with the photoemission lines of Ag $3d_{5/2}$, Au $4f_{7/2}$, and Cu $2p_{3/2}$. The spectra were recorded in constant analyzer energy mode at a pass energy of 160 eV for survey spectra and 40 eV for high-resolution spectra: Mn(2p), C(1s), O(1s), and Li(1s). The survey spectra were summed over 2 scans, and high-resolution spectra were summed over 6 sweeps. In order to avoid X-ray damage on the electrolyte, the spectra of each voltage step: pristine, 4.05 and 4.3 V, were carried out on 3 different grids on the same sample holder, which were all electrically connected. All spectra were energy calibrated using the CF_3 peak in the C 1s at the binding energy of 293.3 eV. The data was evaluated using the CasaXPS software, and the peak fits of all spectra were performed using the Shirley background correction and Gaussian−Lorentzian product formula curve synthesis; 70% Gaussian and 30% Lorentzian.

Density Functional Theory Calculations. DFT calculations apply the VASP code version 5.3,[27−30] the PBE0 functional,[31] and impose a 500 eV energy cutoff. Both the atomic configurations and the dimensions of bulk simulation cells are optimized. The Li_2O, Li_2O_2, LiO_2, $LiMn_2O_4$, $Li_{0.5}Mn_2O_4$, and Li_2CO_3 simulation unit cells have 3, 8, 12, 52, 56, and 96 atoms, and apply 4 × 4 × 4, 5 × 5 × 3, 4 × 4 × 4, 1 × 1 × 1, 1 × 1 × 1, and 1 × 1 × 1 Brillouin zone samplings, respectively. Other details are given in the Results section.

RESULTS

$LiMn_2O_4$. Cyclic voltammetry of the material tested is shown in Figure S1 and is consistent with reported literature. *In situ* potentiostatic delithiation and lithiation steps were performed at 4.05, 4.3, 4.6, and 0.1 V using 10 wt % $LiBF_4$ dissolved in EMI-BF_4 electrolyte. The total integrated charge and discharge capacities are 0.007 mAh and 0.006 mAh. Accurate determination of the mass loading is challenging, but our preparation procedure results in an average sample mass of 0.053 mg. When cycled as traditional composite electrodes, this LMO powder provided 140 mAh g^{-1}, which is the same order of magnitude as our *in situ* experiments (132 mAh g^{-1}). Some capacity fade is anticipated in the first discharge after overcharging to 4.6 V. AES spectra obtained from a series of LMO particles are shown in Figure 2. The same particles were characterized at each voltage step, such that their evolution could be tracked consistently. Similar experiments have been performed where different particles are characterized at each voltage step. We find similar trends in both data sets, suggesting that the electron beam does not play a role in affecting the reaction pathway of the material. In fact, the spot size of the beam is sufficiently small, that we are unlikely to re-examine the same region of each micron scale particle upon subsequent measurements. Figure 3 plots the concentration of each element at each potential. The standard deviations are plotted as error bars. The LMO particles utilized in this study are mostly faceted, with (100) and (111) faces occurring most frequently (see Figure S2). Reactions on LMO surfaces are reported to be sensitive to crystallographic anisotropy, and thus some variation between individual particles is anticipated.[21,22] Despite small variations in absolute values between different particles, the overall trends are quite consistent. The Li surface concentration decreases from 16% to 10% after delithiation to 4.6 V and approximately returns to initial value during lithiation at 0.1 V. The surface concentrations are not anticipated to necessarily reflect those of the bulk, however the ≈16%

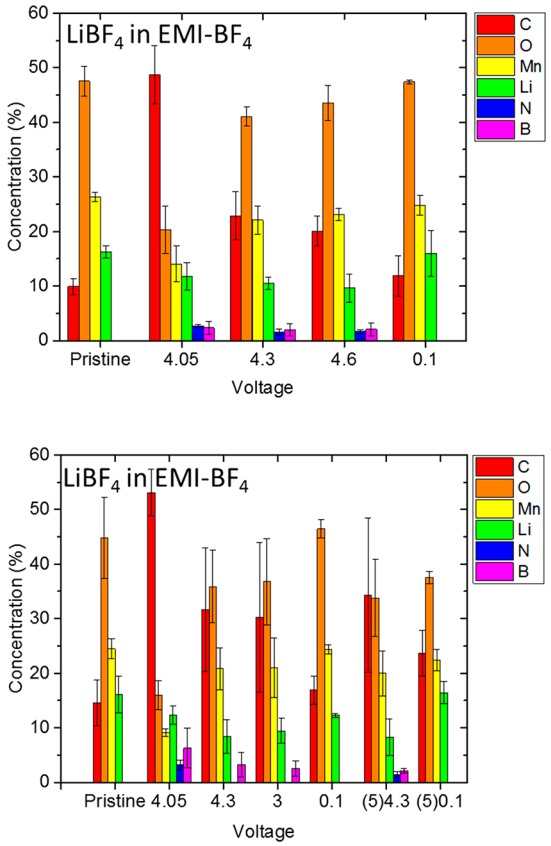

Figure 3. Chemical composition of each element at different voltage steps for samples cycled in EMI-BF_4 electrolyte. The lower plot includes data at 4.3 and 0.1 V after 5 cycles labeled (5).

measured in the pristine and cycled states, is similar to the 14.3% expected for stoichiometric $LiMn_2O_4$. As will be described below, surface Li_2CO_3 accounts for the excess Li measured in the charged state. C concentration varies significantly, increasing from 10% in the pristine state to 49% at 4.05 V. Cycling to higher voltages reduced the C concentration, and upon discharge to 0.1 V the concentration reduces to 12%. Some N and B contamination (<3%) was also observed to reach a maximum concentration at 4.05 V and decrease with increasing voltage. We anticipate that C, N, and B primarily originate as hydrocarbons and/or the low vapor pressure of the electrolyte in the vacuum. The base pressure of the AES before sample introduction was typically $\approx 5 \times 10^{-9}$ Torr before loading the sample and $\approx 1 \times 10^{-8}$ Torr after. If we attributed the excess 5×10^{-9} Torr all to electrolyte vapor and assumed a sticking-coefficient of unity, then a monolayer could form on the order of 8−10 min. Since the concentration of reaction products is significantly less than a monolayer, we posit that the electrode particles are equilibrated at each potential with the species that exists in the vapor phase. We also hypothesize that the carbon can be lost through decomposition into CO or CO_2 and that related oxidation reactions can induce N and B vaporization.

Data was acquired from a second sample tested *in situ* using 10 wt % $LiBF_4$ dissolved in EMI-BF_4 electrolyte (see Figures S3−5). The compositional variations with potential are quite similar across the two samples demonstrating the overall reproducibility of the experiment. Both samples cycled in $LiBF_4$:EMI-BF_4 show minor B and N accumulation on the LMO surfaces at intermediate potentials. This electrolyte also

DOI: 10.1021/acsami.7b10442
ACS Appl. Mater. Interfaces 2017, 9, 33968−33978

contains fluorine, which could react strongly with the surface. However, we observe no distinct F peaks. An estimate of the compositional sensitivity was made by measuring the F composition implied by the experimental noise at the F peak energy, which corresponds to 0.5%. Thus, any F on the surface must be present at compositions below this value.

We performed similar measurements in 10 wt % LiTFSI dissolved in P_{13}TFSI (TFSI electrolyte) cycling between 0.1 and 5 V. This allows us to compare the two different electrolyte chemistries and characterize the effect of severe overcharging. The AES survey and high-resolution spectra can be found in Figures S6–8 and Figures S9–11. The total charge and discharge capacities of the cell cycled to 5.0 V and then 0.1 V were 140 mAh g^{-1} and 50 mAh g^{-1}, respectively. This level of irreversibility is anticipated due to phase transformations induced at high voltages. The total charge and discharge capacities of the cell cycled to 4.6 V and then 3.0 V were 104 and 95 mAh g^{-1}, respectively. This cell is much more reversible as anticipated from the lower overcharging voltage. The chemical compositions associated with cycling two different electrodes, one to 5 V and one to 4.6 V, with LiTFSI:P_{13}TFSI electrolyte are also plotted in Figure 4. Overall, the trends are

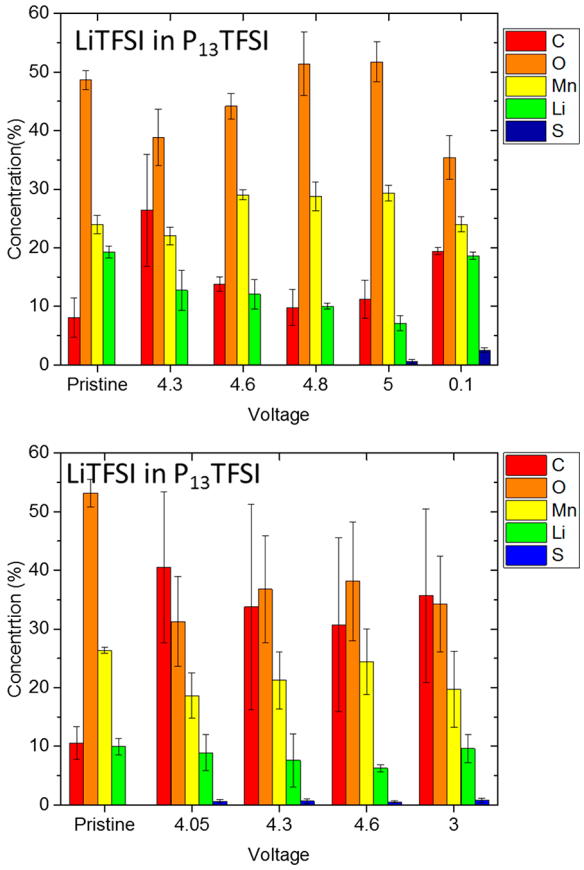

Figure 4. Chemical composition of each element at different voltage steps for samples cycled in P_{13}TFSI electrolyte.

similar for the different experiments. Charging to higher voltages further reduced the C concentration to ≈10% at 4.8 and 5 V. No N or B signal is observed. However, some S is observed, <1% S at 5 V. The observed S should originate from TFSI in the vapor phase, a fact that is supported by the lack of S in the EMI-BF_4 experiments and a lack of B and N in the TFSI experiments. Overall, the trends with regards to the relative compositions are quite similar for LiTFSI:P_{13}TFSI and LiBF_4:EMI-BF_4.

The chemical bonding states of the species observed are of particular interest for understanding the preferred oxidation states and segregation at LMO surfaces as a function of potential. To gain further insight, we compare high-resolution AES data obtained from the standard reference materials such as Mn_2O_3, MnO_2, Li_2O, Li_2CO_3, $MnCO_3$, and our amorphous C film substrate. Complete spectra are provided in Figures S12,13. AES dN/dE peak energies and shapes can be compared and interpreted on a variety of bases.[32−34] Here we take the characteristic peak energy as the most negative peak in the dN/dE signal, which correlates closely with an adsorption edge. Multiple peaks of different energy may overlap and the distance between the maxima and minima dN/dE peak may be considered as a second criteria against which to compare to the reference materials.

Trends in the peak energies of Mn and O as a function of voltage were similar for both electrolytes and are plotted in Figure 5 along with values obtained from the reference spectra. Mn(II) and Mn(III) are difficult to distinguish in terms of both their peak shapes and energies. This is true even in XPS. However, Mn(IV) is observed to shift the Mn LMM peak to lower kinetic energies relative to Mn(II) and Mn(III). For the *in situ* experiments, the pristine LMO material in all samples had the same initial peak energies, thus we conclude the spectra are well aligned and interpret difference >1 eV are chemically meaningful. In the pristine state, the Mn peak sits at 581 eV. Charging in LiBF_4:EMI-BF_4 electrolyte to 4.05 V shifts the peak to a lower kinetic energy of 580 eV. This is consistent with the anticipated oxidation that occurs during the Li^+ extraction. At this potential, O also shifts to lower kinetic energy to 506 eV. The C peak, on the other hand, shifts to higher kinetic energies; from 266.5 eV in the pristine state to 267.3 at 4.05 V. Our reference spectrum has the Li_2CO_3 C peak at 267.5 eV and the O peak at 506 eV. The C and O peaks for $MnCO_3$ fall at 270 and 507.5 eV, respectively, and the O peak for MnO_2 also falls at 507.5. This leads us to conclude that the surface chemistry at 4.05 V is dominated by Li_2CO_3 like bonding and Mn at least partially present as Mn (IV). At 4.3 V, the C concentration is reduced from 49% to 23% and the Mn, O, and C peaks shift to 581, 508, and 267.5 eV. The C peak is still consistent with surface Li_2CO_3, but the Mn peaks in some of the spectra are at slightly higher kinetic energies relative to 4.05 and 4.6 V. At 4.3 V, we interpret the O peak as having contributions from both Li_2CO_3 and $Li_xMn_2O_4$, mostly bonded with Mn(IV). We note that the amount of scatter in the data and the size of the error bars is largest at 4.05 and 4.3 V, where the surface composition is very sensitive to potential. The larger error suggests more particle to particle variation in surface chemistry occurs in this regime. Charging to 4.6 V shifts the Mn peak energy to 589 eV, closer to Mn(IV), the O shifts to 505.2 eV, and the C shifts most dramatically to 265.4 eV. The low kinetic energy associated with the carbon peak has been observed for transition metal carbides.[35] It is difficult to definitively assign a dominant chemistry to the surface at this potential without manganese carbide reference samples. However, we hypothesize that the continuous shift to lower kinetic energies with increasing potential is associated with an increase in the ratio of metal−carbon to metal−carbonate bonding. Surface carbon being present primarily as metal-carbide, rather than carbonate, may explain why TEM-based investigations did not observe a surface carbonate layer during severe overcharging.[17] The

DOI: 10.1021/acsami.7b10442
ACS Appl. Mater. Interfaces 2017, 9, 33968−33978

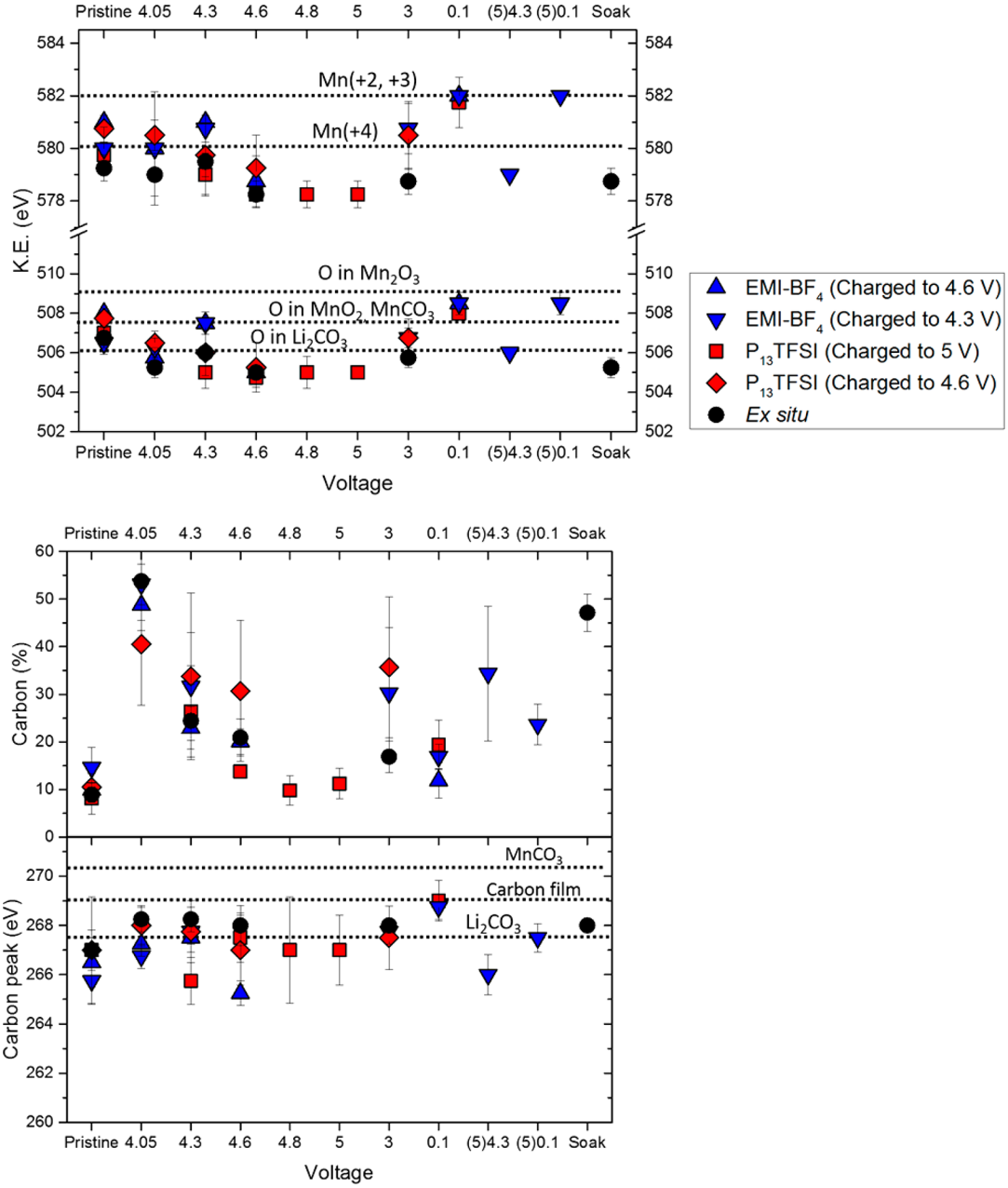

Figure 5. Plots of the peak energies of Mn, O, and C as a function of voltage along with values obtained from the reference spectra. The data labeled (5) were cycled 5 times and the data labeled "Soak" were measured after soaking *ex situ* in commercial electrolyte.

surface concentration of Li is relatively stable at and above 4.3 V despite both delithiation and Li_2CO_3 decomposition, which suggests Li_xO remains on the surface as a decomposition product. Upon lithiating to 3.0 V, the Mn and O peaks are consistent with the pristine $LiMn_2O_4$ material as anticipated from the reversible electrochemical reaction in this voltage range. The C concentration is larger than the pristine material suggesting an accumulation of surface Li_2CO_3 after 1 cycle, which is supported by the C peak at ≈267.5. Lithiating to 0.1 V shifts the Mn and O peaks back toward values more closely associated with mixed Mn(III) and Mn(II) oxides. The C peak shifts to 268.5 eV, and all samples exhibit C peak energies lying significantly above values anticipated for Li_2CO_3. One sample tested using $LiBF_4$:EMI-BF_4 electrolyte was cycled 5 times before obtaining final Auger electron spectra at 4.3 and 0.1 V. Note that the surface chemistries and peak energies of all elements were equivalent, within experimental error, between the first and fifth cycle.

In order to confirm that we can resolve the chemistry of individual particles from the background carbon, we acquired chemical maps of particles at different potentials (see Figure S14). The individual particles are clearly resolved with relatively sharp boundaries between them and the surrounding carbon. The images show the variation in C and Li concentration in the particles as well as an accumulation of some Li and O in the carbon at intermediate potentials, likely as Li_2CO_3, Li_2O, or Li_2O_2. The maps should not be over interpreted compositionally, since they plot the intensity of the peaks in a fixed 1 eV energy window such that a change in intensity may result from either a peak energy shift or a change in composition. Published ^{13}C labeling experiments have shown that some CO and CO_2 originates from material other than the electrolyte, and it was

DOI: 10.1021/acsami.7b10442
ACS Appl. Mater. Interfaces 2017, 9, 33968−33978

hypothesized that oxidation of C conductive additive could be the source.[36] Our mapping of Li and O on the C support generally agrees with this prior finding.

The *in situ* AES results at 4.3 V were somewhat ambiguous with concern to the Mn oxidation state, which derives from a significant amount of experimental variation in the data at this potential. To clarify this point and as shown in Figure 6, we

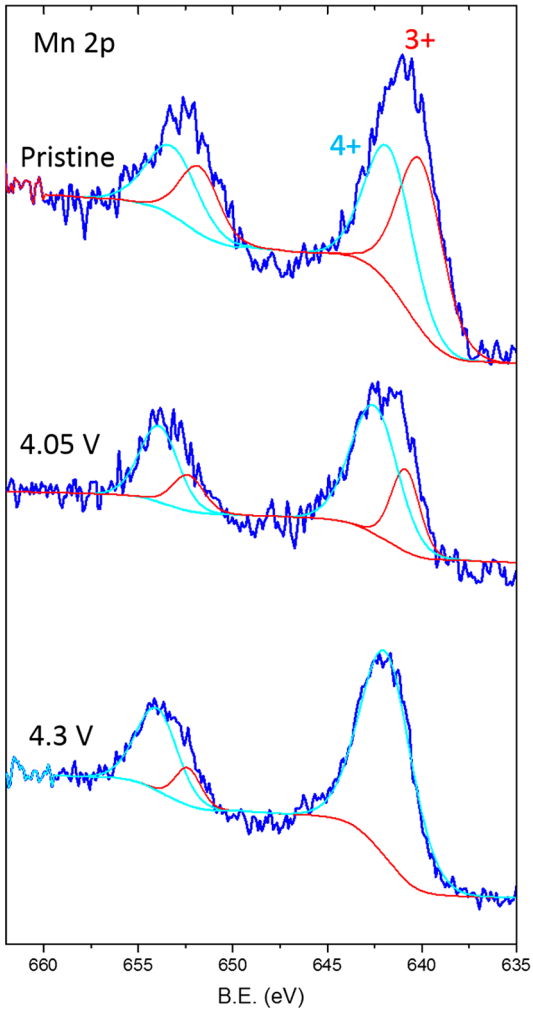

Figure 6. *In situ* XPS Mn 2p spectra obtained at different state of charge: pristine, 4.05, and 4.3 V.

applied *in situ* XPS to the determination of the average oxidation state of Mn in the pristine state ($Mn^{3.5+}$), at 4.05 V ($Mn^{3.72+}$), and at 4.3 V ($Mn^{3.94+}$). These were measured from the Mn 2p, but similar trends are observed for the Mn 3p, shown in Figure S16. The values at each condition correspond well with the anticipated bulk oxidation states at these potentials. The results confirm that Mn(IV) dominates at 4.3 V. The variation and scatter in the Mn AES peak positions at 4.3 V may result from either S contamination and/or electronic structure effects in the doubly ionized material, which can be difficult to interpret. The *in situ* XPS survey scans as well as the Li 1s, O 1s, and C 1s scans are shown in Figures S15−18. The data are consistent with the AES maps in that charging to 4.05 V decreases the total amount of Li in the sample, but increases the Li_2CO_3 concentration. By 4.3 V the Li_2CO_3 concentration decreases, but the changes in concentrations exceed what can be attributed to LMO and are more characteristic of surface reactions occurring on the C support. This fact highlights the benefit of using *in situ* AES to characterize single particles. The variation in C surface concentration with potential also underscores why performing *ex situ* XPS on traditional composite electrodes may not provide reliable information about the bonding states between the active material, O, Li, and C.

A goal of this study is to correlate trends observed from our *in situ* experiments performed under model UHV conditions, with the behavior of real batteries in commercial electrolyte. The observed Li_2CO_3 formation and decomposition as a function of potential measured from our model *in situ* electrochemical cell agree well with those measured by Matsui et al.[18] using *in situ* FTIR in EC:DEC electrolyte. To enable more direct correlation between our *in situ* measurements and the behavior of conventional and commercially relevant cells, we present *ex situ* AES data obtained from LMO composite electrodes cycled in EC-DMC 1 M $LiPF_6$. While brief exposure to atmosphere could modify the surface oxidation states and O concentrations, we anticipate that the overall C concentrations should not be dramatically affected. Figure 7 plots the

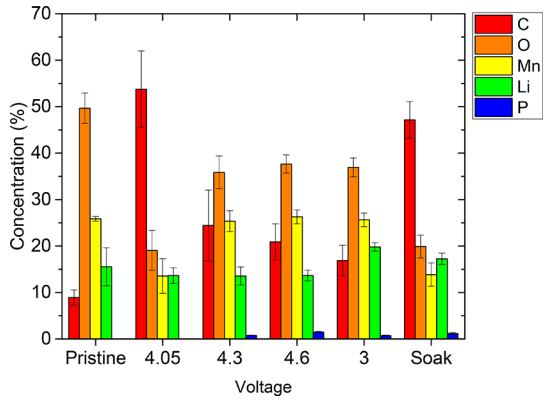

Figure 7. Chemical composition of each element at different voltage steps for samples cycled *ex situ* in commercial electrolyte.

compositions of electrodes charged to different potentials measured by *ex situ* AES, and Figures S19−21 plot the AES survey and high-resolution spectra. The compositional variations closely mirror those measured *in situ*. The material cycled *ex situ* contains a small amount of P (≈1.5%) at potentials >4.3 V, presumably due to a reaction with $LiPF_6$. During charging, the C compositions and chemical shifts match those from the *in situ* experiments well within experimental error (see Figure 5). Discharging *ex situ* at 3 V produces a slightly lower C surface composition; however, the peak energy remains consistent with the *in situ* data. The *ex situ* cycled samples were also compared with material soaked in electrolyte but not cycled. All of the compositions and peak energies of the samples soaked in electrolyte were approximately equivalent to the material cycled to 4.05 V. We hypothesize that during soaking in electrolyte LMO oxidizes the electrolyte in a manner similar to the *ex situ* cell at 4.05 and the oxidation of gaseous species that occurs in the *in situ* cell at 4.05 V. The subtle differences between purely chemical reactions associated with LMO resting in atmosphere or vacuum versus electrolyte indicate that C chemical potential plays a role in organic oxidation under these conditions. However, at higher potentials the differences become negligible. The Mn peaks for the samples cycled *ex situ* were all consistently at higher kinetic

DOI: 10.1021/acsami.7b10442
ACS Appl. Mater. Interfaces 2017, 9, 33968−33978

energies than material cycled *in situ*. It is possible that Mn surface chemistry, bonding, and oxidation state are modified by brief exposure to atmosphere during the *ex situ* tests. This is the inherent problem associated with *ex situ* surface characterization; namely it is unclear to what extent the material is modified during exposure to air. Even short-term storage of exposed samples to the 10^{-6} levels of O_2 and H_2O in a dry glovebox could introduce uncertainty in the analysis.

The variations in surface chemistry and surface bonding information are quite complex. Here we seek to rationalize the observed trends in surface chemistry as a function of potential, by comparing them with potential dependent trends predicted from density functional theory. While surface thermodynamics can differ somewhat from the bulk, we utilize bulk predictions to guide our analysis of the data. In previous work, we have shown that the reaction;

$$Li_2CO_3 \rightarrow CO_2 + 1/2O_2 + 2Li(s) \quad (1)$$

requires a 4.14 eV energy input per Li released at $T = 0$ K.[23] This implies that the oxidation of Li_2CO_3 occurs at or about 4.14 eV vs $Li^+/Li(s)$. The calculation applies the PBE functional which overestimates the O_2 binding energy by about 0.42 eV; this would make the voltage higher. But it ignores the large entropy associated with gas release, which would be larger than 0.42 eV in magnitude under standard state (1.0 atm pressure) conditions, and lower the voltage needed for the reaction. Since CO_2 and O_2 would be continuously consumed and the enclosed battery is not at equilibrium, the precise voltage needed has some uncertainty. Nevertheless, this prediction of CO_2 evolution appears in agreement with the Li_2CO_3 decomposition voltage reported at Li–air battery cathodes.[37] Note that little or no O_2 gas is found to release at low voltages.

For this work, the following reactions relevant to our system were calculated;

$$Li_2CO_3 + 4Li_{0.5}Mn_2O_4 \rightarrow 4LiMn_2O_4 + CO_2 + 1/2O_2 \quad (2)$$

$$Li_2CO_3 + 3Li_{0.5}Mn_2O_4 \rightarrow 3LiMn_2O_4 + CO_2 + 1/2LiO_2 \quad (3)$$

$$Li_2CO_3 + 2Li_{0.5}Mn_2O_4 \rightarrow 2LiMn_2O_4 + CO_2 + 1/2Li_2O_2 \quad (4)$$

They represent the oxidation of Li_2CO_3 by the Mn(IV) → Mn(III) redox reaction, accompanied by the removal of 2, 1.5, and 1 electron for each Li_2CO_3 unit. At $T = 0$ K, the energy change of these three reactions are −0.42, +0.44, +0.95 eV, respectively. If finite temperature entropy gain associated with CO_2 release is included, eq 2 remains favorable and eq 3 would become almost thermoneutral. Although we have not pinpointed the voltage range associated with lithation of $Li_{0.5}Mn_2O_4$ to $LiMn_2O_4$, the favorable or almost thermoneutral oxidation of lithium carbonate with high LMO charge state is consistent with the measurements. Note that the Li_2O_2 and (cubic) Li_2O_2 structures are taken from ref 38 and references therein.

DFT calculations of bulk phase energetics like those described above do not predict the formation of $MnCO_3$. It is likely that Mn(II) forms more readily on surfaces than in bulk LMO, as a result of LMO disproportionation. Indeed, recent computational[23] and experimental[39] studies have strongly suggested the existence of Mn(II) at the electrode/liquid electrolyte interface.

$LiFePO_4$. To demonstrate that the observed chemical reactions are sensitive to cathode chemistry, we also cycled $LiFePO_4$ (LFP) to voltages similar to those utilized for $LiMn_2O_4$. Figure 8 plots the evolution of surface chemistry at different potentials. The Li KLL peaks are obscured by the Fe LMM peaks, so the data does not include this species. Our primary interest in this data relates to the nature of the

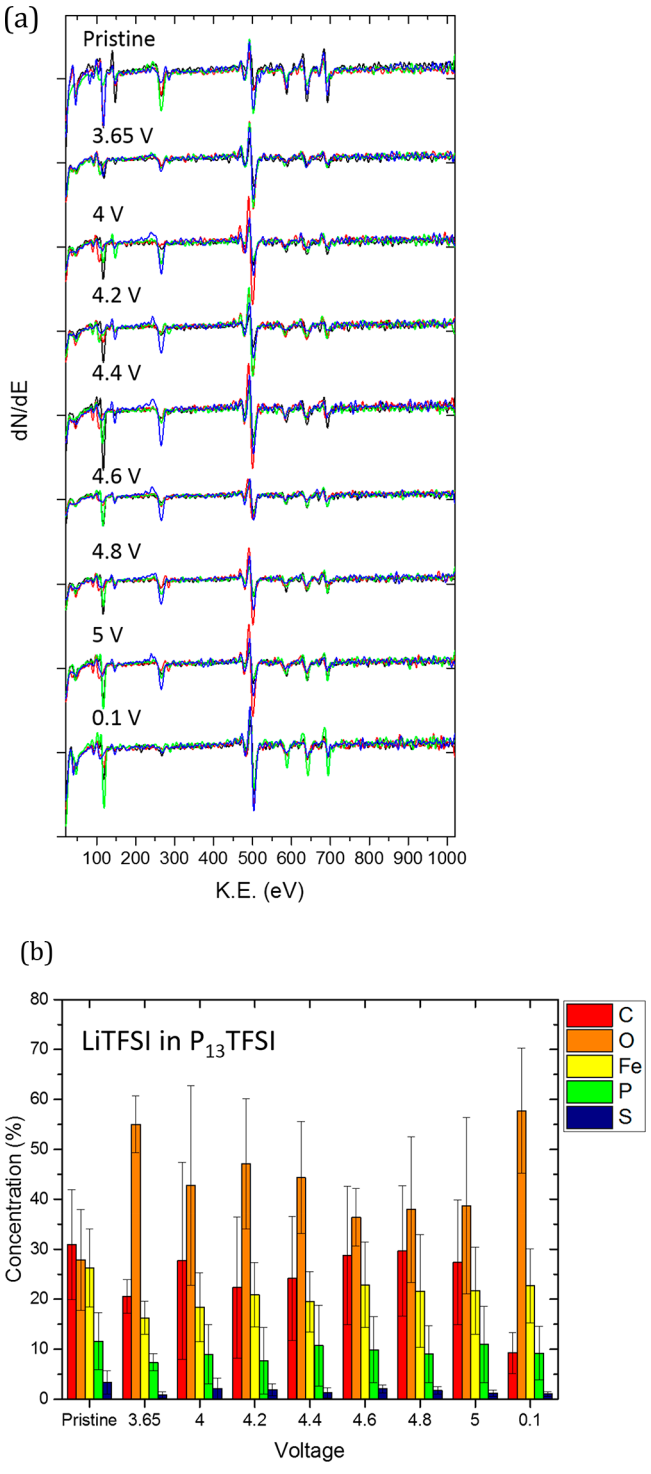

Figure 8. (a) $LiFePO_4$ AES spectra obtained at different potentials. Each line represents a distinct particle. (b) Chemical composition of each element at different voltage steps for samples cycled in $P_{13}TFSI$ electrolyte.

DOI: 10.1021/acsami.7b10442
ACS Appl. Mater. Interfaces 2017, 9, 33968–33978

interaction between C and $LiFePO_4$. Charging to 3.65 V changes the concentrations of all elements most significantly; the C concentration reduces by ≈1/3, the O concentrations increases by a factor of 2, and a 38% reduction in Fe. This charging step corresponds to the electrode going from nominally fully lithiated to almost completely delithiated. Charging to high voltages has little effect on the compositions of the elements outside of the experimental error. The peak energies of Fe, O, C, and P are plotted in Figure 9. A detailed analysis of all the peak energies is outside of the scope of this work, in which we seek to compare the C surface chemistry of $LiFePO_4$ to that of $LiMn_2O_4$. The C KLL peak kinetic energies vary between 264.5 and 265.5 eV up to 4.4 V, and range from 265 to 266 eV up to 5.0 V. These values are all too low to correspond to Li_2CO_3, which is consistent with the fact that the overall C peak shapes do not correspond well to those of Li_2CO_3. Discharging to 0.1 V decreases the C concentration by 18% and increases the O concentration by a comparable amount. This corresponds with relithiation, where the presence of surface Li should favor an accumulation of surface O. At this point, the C peak shifts to 268 eV, which may correspond better to Li_2CO_3 like chemistry. The distinct differences between LFP and LMO demonstrate that the reactions described in detail for LMO are characteristic of that specific chemical system. This is best highlighted by the fact that the C/Fe is almost constant throughout charging, while the C/Mn ratio in LMO varies dramatically during charging.

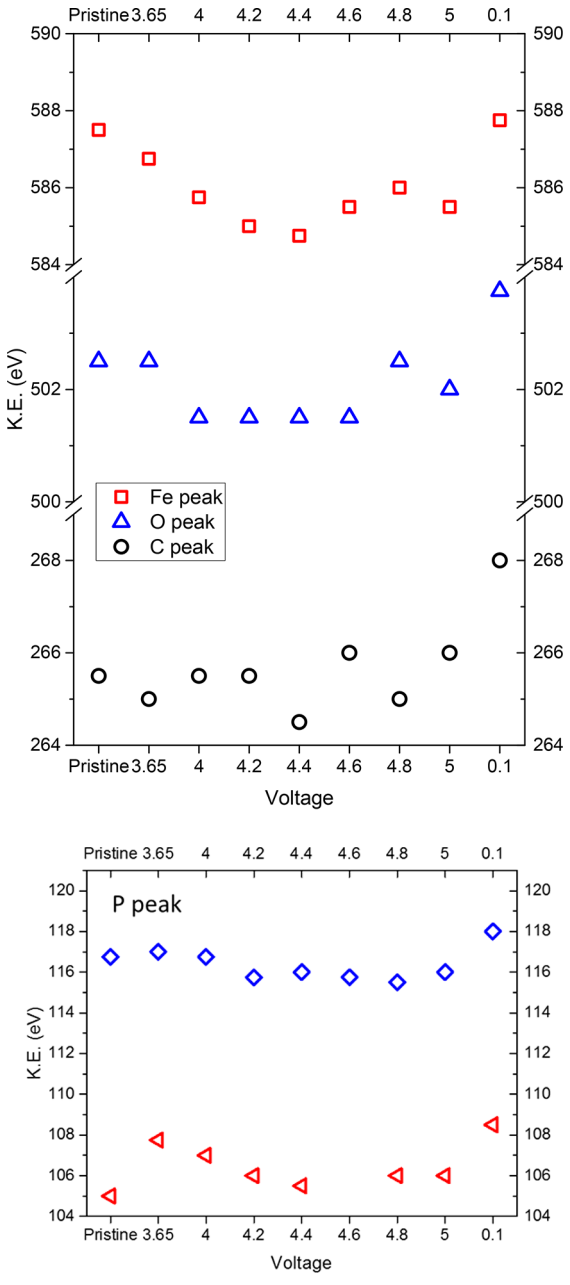

Figure 9. AES characteristic peak energies measured for Fe, O, C, and P as a function of potential averaged over all of the particles.

DISCUSSION

This work characterizes the evolution of LMO surface chemistry equilibrated at different potentials *in situ* in UHV containing the vapor pressures of LiTFSI:P_{13}TFSI and $LiBF_4$:EMI-BF_4 ionic liquid electrolytes. During charging Li_2CO_3 formation becomes favorable on the surface. A peak C/Mn ratio of 3.5 occurs at 4.05 V and decreases with increasing potential. Bulk thermodynamics from DFT predict Li_2CO_3 will tend to decompose above ≈4.14 V. Consistent with this calculation, we find a decreasing C concentration as potential is increased to 4.2 V and greater. The results are similar to those obtained from *in situ* FTIR that observed a rapid increase in carbonate concentration above 3.9 V, a peak at 4.2 V, and a decrease at higher voltages.[18] Measurements of gas evolved from the cathode alone indicate that CO_2 is the most abundant (≈75%), CO is less abundant (≈23%), and C_2H_4 is limited (≈2%).[40] These measurements suggest that the initial electrolyte decomposition and Li_2CO_3 formation occurs through a reaction between its alkyl group and $LiMn_2O_4$, which leads to the release CO/CO_2 and protons. This picture corresponds with our results indicating the presence of carbonate molecules in the electrolyte is not a prerequisite for the formation of a carbonate-based cathode SEI on LMO. Our results suggest that different organic molecules lead to similar Li_2CO_3 formation and decomposition upon charging. This is supported by the fact that our *ex situ* AES data obtained from commercial electrolyte exhibited very similar trends in C composition and bonding as our *in situ* data.

We compared the surface chemistry of $LiMn_2O_4$ in the charged and discharged states after different degrees of overcharging. It is well-known that during severe overcharging the near surface chemistry and crystal structure is irreversibly altered.[17] Nevertheless, electrodes that were initial charged to 5.0 and 4.6 V exhibited nearly identical surface chemistry upon discharging to 3.0 V or severely overdischarging to 0.1 V. Similarly, after overdischarging, which also induces irreversible structural changes, the surface chemistry returns to similar states in the charged, 4.3 V, and discharged states, 0.1 V, even after 5 such cycles. Therefore, the surface chemistry of LMO is highly reversible exhibiting Li_2CO_3 formation and decomposition that is very sensitive to potential.

The behavior of LMO was contrasted against that of LFP. The surface composition and chemistry is relatively stable even to high degrees of overcharging. The results are consistent with *in situ* FTIR, which found that electrolyte decomposition did not occur on LFP until 4.5 V.[41] These values are similar to impedance measurements where a resistance attributed to LFP cathode SEI only increases appreciably at 4.5 V.[42] It should be noted though, that the onset of electrolyte decomposition on Pt electrodes also occurred at similar voltages.[18] Our experiments

DOI: 10.1021/acsami.7b10442
ACS Appl. Mater. Interfaces 2017, 9, 33968−33978

on LFP do not observe significant compositional changes in this regime suggesting the surface does not react with organics in the vacuum. In our testing configuration, the formation of carbonate requires O from the cathode particle. The O in the polyanionic phosphate is less likely to react to form carbonate than the O anions in the oxide. In fact, cathode SEI on $LiFePO_4$ is not well reported and its formation is not facile even at large overpotentials. This leads us to hypothesize that O near the LMO surface participates in C redox and is the major driving force for cathode SEI formation on lithium metal oxides.

The practical implications of the cyclic nature of carbonate formation and decomposition on LMO upon cycling are significant. Within a typical cycling range of 3.0 to 4.3 V, LMO exhibits significant instability in its surface chemistry. The cyclic formation and decomposition Li_2CO_3 will not only degrade the electrolyte, but will also lead to unfavorable gas evolution in the cell. If this behavior is inherent to LMO in a broad range of organic electrolytes, then it will be challenging to chemically avoid capacity fade of LMO even when the Mn(II) dissolution reaction is suppressed. Coating LMO with relatively electrochemically inactive films such as MgO or Al_2O_3 extend the cycle life of this material.[43,44] In fact, such coatings are effective in improving cycle life across a broad range of cathode materials.[45,46] For Al_2O_3-coated LMO, no surface carbonate was observed via *ex situ* XPS.[43] The suppression of surface carbonate formation and dissolution could play an important role in affecting cycle life.

CONCLUSIONS

AES and XPS performed *in situ* with electrochemical cycling was utilized to study the chemistry of $LiMn_2O_4$ surfaces equilibrated in UHV at different potentials. The concentration of surface carbon varies significantly with potential, increasing during charging to 4.05 V and then decreasing at higher overcharging voltages. Discharging to 3.0 V increases the carbon concentration, which is found to again decrease during severe overdischarge to 0.1 V. The AES peak energies and thermodynamics predicted from DFT were utilized to interpret the dominant surface reactions. In the typical cycling range between 4.3 and 3.0 V, surface C tends to form Li_2CO_3. In this regime, Mn primarily undergoes the anticipated redox between Mn(III) and Mn(IV). During overcharging to 5.0 V, C tends to form metal−carbon bonds. Similar results were obtained for both *in situ* and *ex situ* experiments. Finally, $LiMn_2O_4$ was compared with $LiFePO_4$. The two chemistries exhibit very different trends, which demonstrates that the reactions on the $LiMn_2O_4$ surfaces are characteristic of the material.

ASSOCIATED CONTENT

Supporting Information

The Supporting Information is available free of charge on the ACS Publications website at DOI: 10.1021/acsami.7b10442.

Cyclic voltammetry of LMO (Figure S1), SEM image of LMO (Figure S2), *in situ* AES spectra (Figures S3−13), chemical composition mapping (Figure S14), *in situ* XPS spectra (Figures S15−18), *ex situ* AES spectra (Figures S19−21) (PDF)

AUTHOR INFORMATION

Corresponding Author

*S. J. Dillon. E-mail: sdillon@illinios.edu.

ORCID

Ching-Yen Tang: 0000-0002-8003-6825
Kevin Leung: 0000-0003-1397-3752
Richard T. Haasch: 0000-0001-9479-2595

Notes

The authors declare no competing financial interest.

ACKNOWLEDGMENTS

S.D. and C.T. acknowledge support from National Science Foundation under Grant No. 1254406. K.L. is supported by supported by Nanostructures for Electrical Energy Storage (NEES), an Energy Frontier Research Center funded by the U.S. Department of Energy, Office of Science, Office of Basic Energy Sciences under Award Number DESC0001160. Sandia National Laboratories is a multimission laboratory managed and operated by National Technology and Engineering Solutions of Sandia, LLC, a wholly owned subsidiary of Honeywell International, Inc., for the U.S. Department of Energy's National Nuclear Security Administration under contract DE-NA0003525. This work was carried out in part at the Materials Research Laboratory Central Research Facilities, University of Illinois.

REFERENCES

(1) Goodenough, J. B.; Park, K.-S. The Li-Ion Rechargeable Battery: A Perspective. *J. Am. Chem. Soc.* **2013**, *135* (4), 1167−1176.
(2) Thackeray, M. M.; Wolverton, C.; Isaacs, E. D. Electrical energy storage for transportation-approaching the limits of, and going beyond, lithium-ion batteries. *Energy Environ. Sci.* **2012**, *5* (7), 7854−7863.
(3) Arico, A. S.; Bruce, P.; Scrosati, B.; Tarascon, J.-M.; van Schalkwijk, W. Nanostructured materials for advanced energy conversion and storage devices. *Nat. Mater.* **2005**, *4* (5), 366−377.
(4) Lee, E.-S.; Huq, A.; Chang, H.-Y.; Manthiram, A. High-Voltage, High-Energy Layered-Spinel Composite Cathodes with Superior Cycle Life for Lithium-Ion Batteries. *Chem. Mater.* **2012**, *24* (3), 600−612.
(5) Zhu, M.; Park, J.; Sastry, A. M. Fracture Analysis of the Cathode in Li-Ion Batteries: A Simulation Study. *J. Electrochem. Soc.* **2012**, *159* (4), A492−A498.
(6) Wang, D.; Wu, X.; Wang, Z.; Chen, L. Cracking causing cyclic instability of LiFePO4 cathode material. *J. Power Sources* **2005**, *140* (1), 125−128.
(7) Lim, M.-R.; Cho, W.-I.; Kim, K.-B. Preparation and characterization of gold-codeposited LiMn2O4 electrodes. *J. Power Sources* **2001**, *92* (1−2), 168−176.
(8) Wang, H.; Jang, Y. I.; Huang, B.; Sadoway, D. R.; Chiang, Y. M. TEM Study of Electrochemical Cycling-Induced Damage and Disorder in LiCoO2 Cathodes for Rechargeable Lithium Batteries. *J. Electrochem. Soc.* **1999**, *146* (2), 473−480.
(9) Aoshima, T.; Okahara, K.; Kiyohara, C.; Shizuka, K. Mechanisms of manganese spinels dissolution and capacity fade at high temperature. *J. Power Sources* **2001**, *97*−*98*, 377−380.
(10) Kong, W.; Li, H.; Huang, X.; Chen, L. Gas evolution behaviors for several cathode materials in lithium-ion batteries. *J. Power Sources* **2005**, *142* (1−2), 285−291.
(11) Browning, K. L.; Baggetto, L.; Unocic, R. R.; Dudney, N. J.; Veith, G. M. Gas evolution from cathode materials: A pathway to solvent decomposition concomitant to SEI formation. *J. Power Sources* **2013**, *239*, 341−346.
(12) Aurbach, D.; Gamolsky, K.; Markovsky, B.; Salitra, G.; Gofer, Y.; Heider, U.; Oesten, R.; Schmidt, M. The Study of Surface Phenomena Related to Electrochemical Lithium Intercalation into Li x MO y Host Materials (M = Ni, Mn). *J. Electrochem. Soc.* **2000**, *147* (4), 1322−1331.
(13) Cherkashinin, G.; Nikolowski, K.; Ehrenberg, H.; Jacke, S.; Dimesso, L.; Jaegermann, W. The stability of the SEI layer, surface composition and the oxidation state of transition metals at the

electrolyte-cathode interface impacted by the electrochemical cycling: X-ray photoelectron spectroscopy investigation. *Phys. Chem. Chem. Phys.* **2012**, *14* (35), 12321−12331.
(14) Lee, Y.-M.; Nam, K.-M.; Hwang, E.-H.; Kwon, Y.-G.; Kang, D.-H.; Kim, S.-S.; Song, S.-W. Interfacial Origin of Performance Improvement and Fade for 4.6 V LiNi0.5Co0.2Mn0.3O2 Battery Cathodes. *J. Phys. Chem. C* **2014**, *118* (20), 10631−10639.
(15) Gauthier, M.; Carney, T. J.; Grimaud, A.; Giordano, L.; Pour, N.; Chang, H.-H.; Fenning, D. P.; Lux, S. F.; Paschos, O.; Bauer, C.; Maglia, F.; Lupart, S.; Lamp, P.; Shao-Horn, Y. Electrode−Electrolyte Interface in Li-Ion Batteries: Current Understanding and New Insights. *J. Phys. Chem. Lett.* **2015**, *6* (22), 4653−4672.
(16) Lei, J.; Li, L.; Kostecki, R.; Muller, R.; McLarnon, F. Characterization of SEI Layers on LiMn2O4 Cathodes with In Situ Spectroscopic Ellipsometry. *J. Electrochem. Soc.* **2005**, *152* (4), A774−A777.
(17) Amos, C. D.; Roldan, M. A.; Varela, M.; Goodenough, J. B.; Ferreira, P. J. Revealing the Reconstructed Surface of Li[Mn2]O4. *Nano Lett.* **2016**, *16* (5), 2899−2906.
(18) Matsui, M.; Dokko, K.; Kanamura, K. Surface Layer Formation and Stripping Process on LiMn2O4 and LiNi1/2Mn3/2O4 Thin Film Electrodes. *J. Electrochem. Soc.* **2010**, *157* (2), A121−A129.
(19) Yang, L.; Takahashi, M.; Wang, B. A study on capacity fading of lithium-ion battery with manganese spinel positive electrode during cycling. *Electrochim. Acta* **2006**, *51* (16), 3228−3234.
(20) Dai, Y.; Cai, L.; White, R. E. Capacity Fade Model for Spinel LiMn2O4 Electrode. *J. Electrochem. Soc.* **2013**, *160* (1), A182−A190.
(21) Leung, K. First-principles modeling of the initial stages of organic solvent decomposition on Li xMn 2O 4(100) surfaces. *J. Phys. Chem. C* **2012**, *116* (18), 9852−9861.
(22) Kumar, N.; Leung, K.; Siegel, D. J. Crystal Surface and State of Charge Dependencies of Electrolyte Decomposition on LiMn2O4 Cathode. *J. Electrochem. Soc.* **2014**, *161* (8), E3059−E3065.
(23) Leung, K. First-Principles Modeling of Mn(II) Migration above and Dissolution from LixMn2O4 (001) Surfaces. *Chem. Mater.* **2017**, *29*, 2550−2562.
(24) Tang, C.-Y.; Dillon, S. J. In Situ Scanning Electron Microscopy Characterization of the Mechanism for Li Dendrite Growth. *J. Electrochem. Soc.* **2016**, *163* (8), A1660−A1665.
(25) Tang, C.-Y.; Haasch, R. T.; Dillon, S. J. In situ X-ray photoelectron and Auger electron spectroscopic characterization of reaction mechanisms during Li-ion cycling. *Chem. Commun.* **2016**, *52* (90), 13257−13260.
(26) Nandasiri, M. I.; Camacho-Forero, L. E.; Schwarz, A. M.; Shutthanandan, V.; Thevuthasan, S.; Balbuena, P. B.; Mueller, K. T.; Murugesan, V. In Situ Chemical Imaging of Solid-Electrolyte Interphase Layer Evolution in Li−S Batteries. *Chem. Mater.* **2017**, *29* (11), 4728−4737.
(27) Kresse, G.; Furthmüller, J. Efficient Iterative Schemes for Ab Initio Total-Energy Calculations Using a Plane-wave Basis Set. *Phys. Rev. B: Condens. Matter Mater. Phys.* **1996**, *54*, 11169−11186.
(28) Kresse, G.; Furthmüller, J. Efficiency of Ab-initio Total Energy Calculations for Metals and Semiconductors using a Plane-Wave Basis Set. *Comput. Mater. Sci.* **1996**, *6*, 15−50.
(29) Kresse, G.; Joubert, D. From Ultrasoft Pseudopotentials to the Projector Augmented-Wave Method. *Phys. Rev. B: Condens. Matter Mater. Phys.* **1999**, *59*, 1758−1775.
(30) Paier, J.; Marsman, M.; Kresse, G. Why Does the B3LYP Hybrid Functional Fail for Metals? *J. Chem. Phys.* **2007**, *127*, 024103.
(31) Adamo, C.; Barone, V. Towards Reliable Density Functional Methods without Adjustable Parameters: the PBE0Model. *J. Chem. Phys.* **1999**, *110*, 6158−6170.
(32) Sault, A. G. Quantitative analysis of Auger lineshapes of oxidized iron. *Appl. Surf. Sci.* **1994**, *74* (3), 249−262.
(33) Szalkowski, F. J.; Somorjai, G. A. Auger electron spectroscopy investigations of the surface chemical composition of vanadium, the vanadium oxides, and oxidized vanadium: Chemical shift and peak intensity analysis. *J. Chem. Phys.* **1972**, *56* (12), 6097−6103.
(34) Hooker, M. P.; Grant, J. T. The use of Auger electron spectroscopy to characterize the adsorption of CO on transition metals. *Surf. Sci.* **1977**, *62* (1), 21−30.
(35) Back, T.; Fairchild, S. B.; Averett, K.; Maruyama, B.; Pierce, N.; Cahay, M.; Murray, P. T. Pulsed-Laser Deposited Transition-Metal Carbides for Field-Emission Cathode Coatings. *ACS Appl. Mater. Interfaces* **2013**, *5* (18), 9241−9246.
(36) Onuki, M.; Kinoshita, S.; Sakata, Y.; Yanagidate, M.; Otake, Y.; Ue, M.; Deguchi, M. Identification of the source of evolved gas in li-ion batteries using 13C-labeled solvents. *J. Electrochem. Soc.* **2008**, *155* (11), A794−A797.
(37) Luntz, A. C.; McCloskey, B. D. Nonaqueous Li-Air Batteries: A Status Report. *Chem. Rev.* **2014**, *114*, 11721−11750.
(38) Lau, K. C.; Curtiss, L. A.; Greeley, J. Density Functional Investigation of the Thermodynamic Stability of Lithium Oxide Bulk Crystalline Structures as a Function of Oxygen Pressure. *J. Phys. Chem. C* **2011**, *115*, 23625−23633.
(39) Qiao, R. W. Y.; Olalde-Velasco, P.; Li, H.; Hu, Y.-S.; Yang, W.; Wang, Y. Direct Evidence of Gradient Mn(II) Evolution at Charged States in LiNi0.5Mn1.5O4. *J. Power Sources* **2015**, *273*, 1120−1126.
(40) Lee, K. H.; Song, E. H.; Lee, J. Y.; Jung, B. H.; Lim, H. S. Mechanism of gas build-up in a Li-ion cell at elevated temperature. *J. Power Sources* **2004**, *132* (1−2), 201−205.
(41) Akita, Y.; Segawa, M.; Munakata, H.; Kanamura, K. In-situ Fourier transform infrared spectroscopic analysis on dynamic behavior of electrolyte solution on LiFePO4 cathode. *J. Power Sources* **2013**, *239*, 175−180.
(42) Liu, Y.; Xie, J. Failure Study of Commercial LiFePO4 Cells in Overcharge Conditions Using Electrochemical Impedance Spectroscopy. *J. Electrochem. Soc.* **2015**, *162* (10), A2208−A2217.
(43) Guan, D.; Jeevarajan, J. A.; Wang, Y. Enhanced cycleability of LiMn2O4 cathodes by atomic layer deposition of nanosized-thin Al2O3 coatings. *Nanoscale* **2011**, *3* (4), 1465−1469.
(44) Lim, S.; Cho, J. PVP-functionalized nanometre scale metal oxide coatings for cathode materials: successful application to LiMn2O4 spinel nanoparticles. *Chem. Commun.* **2008**, *37*, 4472−4474.
(45) Kim, Y. J.; Cho, J.; Kim, T.-J.; Park, B. Suppression of Cobalt Dissolution from the LiCoO2 Cathodes with Various Metal-Oxide Coatings. *J. Electrochem. Soc.* **2003**, *150* (12), A1723−A1725.
(46) Myung, S.-T.; Izumi, K.; Komaba, S.; Yashiro, H.; Bang, H. J.; Sun, Y.-K.; Kumagai, N. Functionality of Oxide Coating for Li[Li0.05Ni0.4Co0.15Mn0.4]O2 as Positive Electrode Materials for Lithium-Ion Secondary Batteries. *J. Phys. Chem. C* **2007**, *111* (10), 4061−4067.

DOI: 10.1021/acsami.7b10442
ACS Appl. Mater. Interfaces 2017, 9, 33968−33978